Journal of Functional Materials and Applied Engineering

Research Paper

Optimization of Preparation Conditions and Characterization of Biochar-Supported Nanoscale Zero-Valent Iron Materials

Lucía Santos [1], Clinton Hussien [1], Chamizo Eugenio [2,*]

[1] University of Lorraine, 27 rue Philippe Seguin , Epinal, 88000 , France
[2] Institute of Forest Science (ICIFOR-INIA), CSIC, Ctra. de la Coruña, km 7,5, Madrid 28040, Spain

*Corresponding author: Chamizo.eugenio@inia.csic.es

Abstract. Tetracycline is a widely used antibiotic worldwide, and its residues in aquatic environments can cause persistent pollution, affect the ecological balance, and be harmful to human health. Fenton-like reaction is a commonly used advanced oxidation method for removing refractory organic pollutants, while nano-zero valent iron is a commonly used and efficient catalyst. In this study, biochar-nano zero valent iron (BC-nZVI) composite materials were prepared from food waste and peanut shells by liquid phase reduction method to construct a BC-nZVI+H_2O_2 Fenton-like system for the degradation of tetracycline in water. The degradation performance of the system, the influence of various experimental conditions, the reaction mechanism, and the catalytic performance and stability of BC-nZVI were investigated. Results of electron paramagnetic resonance (EPR) indicated that hydroxyl radicals were produced in the reaction process, and the material had high catalytic efficiency for hydrogen peroxide. The reaction order n for the decomposition of hydrogen peroxide was 1.0709, and the reaction rate constant k=0.1243 min^{-1}. BC-nZVI materials mainly degraded tetracycline through the synergistic effects of physical adsorption, chemical reduction, and catalytic degradation. The BC-nZVI+H_2O_2 Fenton system had a high degree of mineralization of tetracycline, with a TOC removal rate of 81.63%. Tetracycline was oxidized and hydroxylated under the action of free radicals in the medium, followed by demethylation and methylamino group removal, further ring opening, and degradation into small molecular intermediate products, which eventually decomposed into CO_2 and H_2O.

Keywords: *biochar; BC-nZVI; Fenton-like; Tetracycline*

Received on 15 Sep 2024, Accepted on 15 Oct 2024, Published on 15 Dec 2024

1 Introduction

Fenton reaction is a technology that utilizes hydrogen peroxide decomposition to generate free radicals for pollutant degradation. The Fenton oxidation process has emerged as a highly potent technique for eliminating organic contaminants—particularly those exhibiting resistance to conventional degradation—owing to its exceptional efficacy in target compound destruction, comprehensive mineralization capacity, and minimal generation of harmful byproducts [1]. The incorporation of ferrous ions alongside hydrogen peroxide facilitates the efficient breakdown of numerous recalcitrant organic species prevalent in aquatic matrices, encompassing aromatic hydroxyl compounds and pharmaceutical agents such as tetracycline-class antimicrobials [2]. Relative to alternative advanced oxidation methodologies, this particular approach offers distinct operational benefits: the requisite chemicals demonstrate cost-effectiveness, straightforward manipulability, and convenient storage characteristics, while the transformation occurs under ambient thermal and atmospheric conditions without necessitating specialized equipment. These collective attributes render the methodology particularly attractive for practical implementation in aqueous-phase contaminant abatement applications where economic viability remains a paramount consideration. Based on the phase distribution of the catalytic species, Fenton-based oxidation systems can be broadly classified into two categories: those employing dissolved iron catalysts operating within a single liquid phase, and those utilizing solid-phase iron-containing materials that facilitate

interfacial redox processes.

The specific mechanism is listed as follows: In the first stage, as shown in Equation 1-1, Fe^{2+} can react with hydrogen peroxide under acidic conditions, producing Fe^{3+} and highly oxidative ·OH. When Fe^{3+} is present in the solution, Fe^{3+} continues to react with H_2O_2 and is reduced back to Fe^{2+}. Therefore, under sufficient conditions, continuous reaction of Fe^{2+} can generate more ·OH.

$Fe^{2+} + H_2O_2 \rightarrow Fe^{3+} + \cdot OH + OH^-$

Subsequently, the reaction between ·OH and H_2O_2 produces $HO_2\cdot$ and H_2O, as shown in Equation 1-2. However, the oxidative capacity of $HO_2\cdot$ is weaker than that of ·OH.

Equation 1-2:$\cdot OH + H_2O_2 \rightarrow HO_2\cdot + H_2O$

Fe^{2+} reacts with ·OH to generate Fe^{3+}, as shown in Equation 1-3.

Equation 1-3:$Fe^{2+} + \cdot OH \rightarrow Fe^{3+} + OH^-$

Fe^{3+} further reacts with $HO_2\cdot$ to generate Fe^{2+}. Equations 1-3 and 1-4 indicate that the generation of Fe^{2+} and Fe^{3+} is a cyclic process. When Fe^{2+} reacts again with H_2O_2 to produce ·OH, this cycle continues.

$Fe^{3+} + HO_2\cdot \rightarrow Fe^{2+} + O_2 + H^+$

Conventional Fenton reactions are severely affected by solution pH. Moreover, conventional single-phase Fenton configurations demand stringent pH control—typically below 3—to prevent the formation of insoluble ferric hydroxide precipitates and the consequent accumulation of substantial quantities of iron-rich sludge. This operational constraint mandates considerable chemical inputs for initial acidification and subsequent neutralization, thereby introducing procedural complexity and diminishing overall cost-effectiveness. Although metal-based catalysts often exhibit relatively high catalytic performance, their cost is high, and catalyst recovery is challenging. Furthermore, due to particle aggregation in water, their catalytic activity in reaction systems decreases, highlighting the urgent need to find suitable alternatives. Conversely, solid-phase catalytic systems eliminate the necessity for rigorous acidity regulation and substantially curtail sediment formation; however, mass transfer limitations at the liquid-solid interface considerably impede transformation rates, ultimately compromising contaminant elimination performance. Incorporating materials with nanoscale dimensional features represents a promising refinement tactic, as these architectures intensify surface reactivity and may substantially accelerate the overall degradation trajectory [3,4].

Heterogeneous Fenton reactions typically refer to systems where iron or its compounds are loaded onto a carrier as a solid catalyst, combined with hydrogen peroxide to form a Fenton-like system. This modification facilitates elevated generation of hydroxyl radicals from the peroxide precursor, thereby amplifying the destruction efficacy of antimicrobial compounds. Relative to their homogeneous counterparts, heterogeneous configurations tolerate broader acidity spectra, minimize aqueous iron leaching, and feature streamlined operational protocols with enhanced user convenience. Furthermore, the robust structural integrity of immobilized catalytic phases permits multiple regeneration cycles, contributing to substantial economic savings through diminished material consumption [5]. Thus, heterogeneous Fenton reaction systems composed of such catalysts are a good alternative to homogeneous Fenton systems. To date, they can be mainly classified into three categories: (1) Iron compounds, primarily Fe_2O_3, Fe_3O_4, and iron oxyhydroxides (α-, β-, γ-FeOOH). (2) Other metal oxides, including metals such as Cu, Ti, Co, Mn, which exist in multiple oxidation states and can effectively transfer electrons to H_2O_2 by changing oxidation states, promoting H_2O_2 to produce ·OH for degrading organic pollutants. (3) Metal-organic framework materials, where multiphase Fenton catalysts are loaded on activated carbon, clay, molecular sieves, etc., incorporating other metal ions besides iron to improve reaction rates and catalytic activity [6]. Qin and colleagues [7] fabricated amino-functionalized carbon-supported manganese ferrite nanocomposites through a hydrothermal methodology, subsequently deploying these materials for catalytic peroxide activation in the oxidative degradation of a multi-component pharmaceutical mixture comprising fluoroquinolone, penicillin, and tetracycline derivatives. Following a three-hour treatment period, chemical oxygen demand

abatement reached 63.8%, while the biochemical-to-chemical oxygen demand ratio escalated markedly from 0.012 to 0.36—evidence of substantially improved susceptibility to microbial mineralization and favorable conditions for downstream biological processing stages. Cycling experiments confirmed the durable performance and structural integrity of the amino-decorated carbon-encapsulated spinel ferrite throughout repeated Fenton-like applications. Across six successive operational cycles, the efficiency in chemical oxygen demand reduction exhibited only modest attenuation, declining from 63.8% to 58.4%. In related work, He and collaborators [8] synthesized granular activated carbon impregnated with iron oxide phases, subsequently evaluating its catalytic potential for tetracycline transformation under heterogeneous oxidation conditions. The investigators observed that at an initial acidity of 3.0, the iron-impregnated granular activated carbon-mediated Fenton configuration attained peak elimination efficacy of 92.6%. Assessment of total organic carbon depletion revealed superior mineralization capability for the iron-modified system at 67.2%, representing approximately a 1.3-fold enhancement relative to the unmodified carbon analogue. Elution studies demonstrated distinct mechanistic contributions: for the pristine carbon system, surface accumulation and oxidative breakdown contributed 19.22% and 80.78% respectively to overall tetracycline depletion, whereas the iron-functionalized variant exhibited reduced sorptive uptake (10.58%) coupled with substantially elevated degradation predominance (89.42%).

In recent decades, advanced oxidation processes (AOPs) have been effective solutions for degrading many toxic and persistent pollutants. As a classic AOP, the Fenton method is widely used for treating organic pollutants in water environments due to its high efficiency and environmental friendliness. However, in traditional Fenton systems, ferrous ions are consumed too rapidly, and large amounts of sludge are produced during the coagulation stage. To address this limitation, heterogeneous Fenton-like processes have been developed, where solid-phase activators can be recovered. Recent investigations have explored diverse catalytic initiators, encompassing metallic iron in its elemental state, oxyhydroxide mineral phases, porous carbonaceous matrices, and thermally treated biomass derivatives. Nanostructured materials have demonstrated considerable promise for contaminant attenuation within Fenton-type oxidation frameworks. Specifically, nanodimensional zerovalent iron species function as potent peroxide activators capable of addressing a broad spectrum of environmental pollutants. The diminutive particle dimensions confer expansive interfacial area and exceptional chemical reactivity, enabling sustained ferrous ion liberation under acidic conditions—thereby perpetuating hydroxyl radical formation through redox-mediated peroxide decomposition. The Fe^{3+} produced by these reactions sequentially reacts with Fe^{0}, providing continuous Fe^{2+} for the Fenton-like process, as shown in follows.

$$Fe^{0} + H_2O_2 + 2H^{+} \rightarrow Fe^{2+} + 2H_2O$$

$$Fe^{2+} + H_2O_2 \rightarrow Fe^{3+} + \cdot OH + OH^{-}$$

$$2Fe^{3+} + Fe^{0} \rightarrow 3Fe^{2+}$$

Simultaneously, BC-nZVI composites prepared using biochar as a carrier can effectively reduce nZVI agglomeration and enhance material stability [9]. Iron-based Fenton-like reaction systems refer to systems where iron-based catalysts catalyze H_2O_2 to construct Fenton-like systems, broadening the pH application range, offering simple operating conditions, recyclability, no iron sludge production, and easy solid-liquid separation. As a widely used advanced oxidation reaction, research on Fenton reaction catalysts and system improvements has attracted much attention, particularly regarding iron-based catalyst enhancements. Deng and associates [10] fabricated biochar-supported nanoscale zerovalent iron hybrids through aqueous-phase reductive precipitation, subsequently deploying these constructs as highly efficient peroxide activators within a Fenton-inspired oxidation architecture targeting sulfonamide antimicrobial elimination. Within this integrated platform, the metallic nanoparticles serve as the principal redox mediators driving hydroxyl radical genesis for pharmaceutical breakdown, whereas the carbonaceous scaffold fulfills multiple complementary functions: structural stabilization of the reactive iron phase, concentrative uptake of target contaminants, auxiliary peroxide activation, and suppression of surface oxide layer formation that would otherwise compromise metallic reactivity. The cooperative interplay between these constituents underpins the exceptional efficacy observed for the composite material in sulfonamide abatement applications. Nevertheless, extended operational cycling revealed appreciable performance deterioration, with elimination efficiency declining substantially from 74.04% to 38.02% across three sequential deployments. Gan et al. [11] found that sludge-derived iron-rich biochar can serve as an

effective Fenton catalyst for degrading refractory organic compounds. By pyrolyzing iron-containing sludge cake, biochar rich in multivalent iron was prepared, catalyzing H_2O_2 via homogeneous and heterogeneous reactions to degrade 4-chlorophenol in water. After five uses, the degradation efficiency still reached 100%, showing significant effects. Chen et al. [12] used tea leaves as raw material, prepared Fe_2O_3/BC composites via one-step impregnation pyrolysis under ventilation, and observed uniform distribution of Fe_2O_3 on biochar through material characterization. Dye removal efficiency exceeded 80%, and high catalytic activity was maintained after four uses. Xie et al. [13] synthesized magnetic nanocatalysts (MNCs) using ferric chloride and ferrous chloride via coprecipitation. Under H_2O_2 participation in a Fenton-like system, degradation efficiency for ethidium bromide reached 98.97% under optimal conditions, and 62.17% after five consecutive reaction cycles. Padk et al. [14] prepared iron-modified biochar by impregnating bagasse in ferrous sulfate solution and applied the catalyst in a Fenton-like reaction to remove Orange G from water. After four consecutive uses, 89.3% of Orange G was still removed. It can be seen that after combining with iron, the catalytic performance of biochar is greatly enhanced.

This project uses kitchen waste as raw material to prepare biochar-loaded nZVI via hydrothermal carbonization as a catalyst for H_2O_2, constituting a Fenton-like system, effectively preventing nZVI agglomeration, enabling relatively uniform distribution on the carbon material surface, enhancing catalytic action, and effectively removing tetracycline from water through ·OH produced by the Fenton-like system.

2 Materials and Methods

2.1 Preparation of Biochar by Hydrothermal Carbonization

Biochar was prepared using the hydrothermal carbonization method, which is economical and efficient. The carbonization process of kitchen waste involves reactions mainly including dehydration, deamination, and decarboxylation of polysaccharides. Approximately 8% to 15% of the total solids produce fatty acids, hydrocarbons, ammonia, and aldehydes. The mechanisms of dehydration, deamination, and decarboxylation further convert these substances into many intermediates, such as furans, heterocycles, furfural, carbonaceous amines, aldols, benzene derivatives, and condensed ring aromatic hydrocarbons. Temperature is the core factor controlling material transformation and the structure of surface functional groups of the product. Simultaneously, hydrothermal temperature is closely related to the specific surface area of the material [15,16]. Therefore, to investigate the influence of biochar preparation conditions on material properties, this study produced three types of biochar by varying the residence temperature during preparation for subsequent material synthesis. The specific method is as follows:

Leftover rice and cleaned peanut shells were dried in a blast drying oven for 72 hours, then crushed. Subsequently, 20 g of peanut shells and 80 g of leftover rice were weighed and sequentially added to a reaction vessel. Then, 250 mL of deionized water was measured and poured into the reaction vessel to immerse the solid raw materials. The reaction vessel was sealed, and batch residence temperatures were set at 240°C, 260°C, and 280°C for a residence time of 2 hours. Following thermal treatment completion, the carbonized product was extracted and subjected to sequential purification: triple rinsing with anhydrous ethanol followed by deionized water, subsequent desiccation in a convection oven for forty-eight hours, mechanical pulverization, and final size classification through a 150-μm aperture screen. This protocol yielded three distinct biochar variants prepared at discrete pyrolysis temperatures, maintained in reserve for subsequent experimental utilization.

2.2 Preparation of Biochar-Supported Nanoscale Zero-Valent Iron Material

BC-nZVI material was prepared via the liquid-phase reduction method. As an economical and environmentally friendly method, the reaction occurs in the liquid phase. Sodium borohydride is added to reduce ferric or ferrous ions to zero-valent iron. The reaction process is mild, stable, easy to control, and synthesizes nanoscale zero-valent iron on the biochar surface. The specific reaction mechanism is shown:

$$Fe^{3+} + 3BH_4^- + 9H_2O \rightarrow Fe^0 \downarrow + 3B(OH)_3 + 10.5H_2 \uparrow$$

$$Fe^{3+} + 2BH_4^- + 6H_2O \rightarrow Fe^0 \downarrow + 2B(OH)_3 + 7H_2 \uparrow$$

Zhang et al. [61] found that by changing the ratio of a mixture of soybean and straw powder (carbon source) to iron element, the prepared materials with different loadings showed significant differences in the degradation effect of atrazine in a persulfate oxidation system. When the mass ratio of biochar to iron oxide was 7:1, the best catalytic effect was obtained. Hussain et al. [17] used rice husks as raw material to prepare biochar via pyrolysis. Ferrous sulfate ($FeSO_4 \cdot 7H_2O$) was reacted with sodium borohydride ($NaBH_4$) to load zero-valent iron onto the biochar. Four different materials were prepared by varying the iron-to-carbon ratio to 1:1, 1:2, 1:3, and 1:4. These materials were used to degrade nonylphenol in an oxidation system, and significant differences in effectiveness were found. The highest degradation efficiency of 38.52% was achieved at an nZVI-to-BC ratio of 1:3. Therefore, to explore the effect of the iron-to-carbon ratio on material properties, this study prepared nine different materials by directly varying the iron-to-carbon ratio through changing the amount of biochar added. The specific method is as follows: As shown in Table 3.3, certain amounts of biochar prepared at 240°C, 260°C, and 280°C were weighed and immersed in 80 mL of 0.1 mol/L ferric chloride ($FeCl_3 \cdot 6H_2O$) solution, and left at room temperature for 72 hours. After 72 hours, the mixture was transferred to a three-neck flask, 80 mL of absolute ethanol was added, and N_2 was purged. The blend was agitated for half an hour to establish a homogeneous dispersion. Subsequently, an aqueous sodium borohydride solution (100 mL) was introduced gradually via controlled addition to the vigorously mixed suspension, with the transformation proceeding for an additional thirty-minute interval. After the reaction, centrifugation was performed to remove the supernatant. Deionized water was added for stirring, followed by centrifugation and removal of the supernatant. Ethanol was added, and the same operation was repeated, alternating three times to remove residual $NaBH_4$. The obtained product was vacuum-dried at 60°C for 8 hours, finally preparing nine BC-nZVI composite materials with three different mass ratios (BC:nZVI = 1:3, BC:nZVI = 1:1, BC:nZVI = 3:1) using biochar carriers prepared at different temperatures. As a reference material, unmodified nanoscale zerovalent iron was synthesized through an identical protocol excluding the carbonaceous support. Freshly fabricated specimens of both the biochar-iron composites and the standalone metallic nanoparticles were preserved in airtight containers under refrigerated conditions (4°C) prior to experimental deployment.

2.3 Analytical Methods

2.3.1 Determination of Iron Loading Capacity

The total iron content was determined using the 1,10-phenanthroline spectrophotometric method. 1,10-Phenanthroline can form a complex with Fe^{2+} that has a characteristic peak at 510 nm. The reaction is highly selective, has a wide pH response range, and the relationship between concentration and absorbance obeys the Beer-Lambert law. When iron is in the trivalent state, it can be reduced using hydroxylamine hydrochloride. The reaction formula is shown in Formula 2.3.

$$2Fe^{3+} + 2NH_2OH \cdot HCl \rightarrow 2Fe^{2+} + N_2 \uparrow + 4H^+ + 2H_2O + 2Cl^-$$

Although the color development reaction can proceed within pH = 2–9, values that are too high or too low will adversely affect the reaction, either reducing the reaction rate or causing Fe^{2+} hydrolysis. In this experiment, hydroxylamine hydrochloride was first used to reduce Fe^{3+} to Fe^{2+}, and then the pH was adjusted to 4–5 for the reaction with 1,10-phenanthroline. Iron standard solutions with concentrations of 0, 0.4, 0.8, 1.6, 2.4, 3.2, and 4.0 μg/L were prepared. Absorbance was measured at 510 nm. The standard curve is shown in Formula 2.4, with $R^2 = 0.9992$.

$$y = 0.2169x + 0.0090$$

2.3.2 Total Organic Carbon (TOC) Determination

Total Organic Carbon serves as a direct quantitative metric for carbonaceous content determination through complete oxidative conversion, in contrast to five-day biochemical oxygen demand, permanganate oxidizability, and dichromate oxygen demand—which derive organic loading estimates indirectly via oxygen depletion measurements. Consequently, TOC enables immediate evaluation of organic matter influence on aquatic systems, encompassing recalcitrant substances resistant to biological assimilation. The present investigation employed the extent of carbon diminution in the aqueous phase as the definitive indicator for assessing the degree of tetracycline transformation to inorganic end-products.

2.3.3 Hydrogen Peroxide Concentration Determination

$Ti(SO_4)_2$ and H_2O_2 form a yellow peroxide-titanium complex precipitate, which can be dissolved by sulfuric acid and measured colorimetrically at a wavelength of 415 nm. The higher the hydrogen peroxide concentration, the deeper the color. This method was used to determine changes in hydrogen peroxide content. The standard curve was drawn as follows: 1 mL of 30% H_2O_2 solution was measured and diluted to volume in a 100 mL volumetric flask to prepare a 100 mmol/L H_2O_2 solution. Concentrated sulfuric acid was diluted to prepare a 2 mol/L sulfuric acid solution. A precisely weighed quantity of titanium sulfate was solubilized in 6 mL of concentrated hydrochloric acid within a thermostatically controlled aqueous environment maintained at 60°C, subsequently permitted to equilibrate to ambient thermal conditions before preservation under refrigerated storage (4°C). Different volumes of 100 mmol/L H_2O_2 solution were used to prepare H_2O_2 solutions with concentrations of 1.5, 1.2, 0.8, 0.6, 0.4, 0.2, and 0.1 mmol/L. Then, 1.6 mL of each solution was added to test tubes, followed by 0.16 mL of 5% titanium sulfate solution and 0.32 mL of concentrated ammonia water. The mixture was centrifuged at 8000 r/min to remove the supernatant. Subsequently, 2.4 mL of sulfuric acid (2 mol/L) was introduced to effect dissolution of the solid residue. The resulting liquid phase was carefully decanted into a 10-mL volumetric flask, while the original centrifugation vessel underwent repeated rinsing with purified water—each aliquot of rinse liquid being combined with the primary solution within the volumetric container prior to final dilution to the calibration mark. Absorbance was measured at 415 nm. The standard curve is shown in Formula 2.5, with R^2 = 0.9993.

$$y = 0.3463x + 0.0038$$

2.3.4 Hydroxyl Radical Detection Method

This study used the salicylic acid method to detect hydroxyl radicals. A precisely measured volume of ethanol together with a predetermined mass of salicylic acid was introduced into an Erlenmeyer flask, followed by incremental addition of dilute hydrogen peroxide solution. Subsequently, a quantified amount of the biochar-supported nanoscale zerovalent iron composite was dispersed into the reaction medium, with the entire assembly subjected to continuous orbital agitation at 180 oscillations per minute under thermostated conditions maintained at 20°C. For absorbance measurement, samples were taken every 5 minutes with a disposable syringe and measured in a 10 mm cuvette. A solution without BC-nZVI material was used as the reference. The measured absorbance is directly proportional to the hydroxyl radical content, which is indirectly represented by the absorbance.

2.3.5 Analysis of Degradation Intermediates

Liquid chromatography-mass spectrometry (LC-MS) combines liquid chromatography and mass spectrometry, enhancing the detection and analysis capabilities of samples to some extent, especially for samples with complex matrix conditions. It offers advantages such as higher precision, faster speed, good sensitivity, and the ability to analyze multiple trace compounds simultaneously. Therefore, this study used LC-MS to analyze the possible structures of intermediate products and infer the possible degradation pathway of tetracycline.

2.4 Material Characterization Methods

2.4.1 Scanning Electron Microscopy (SEM)

Scanning Electron Microscopy (SEM) is widely used in nanomaterials research. It can obtain information such as morphology and particle size without preparing a large amount of samples and can collect large-scale structural data at low magnification. SEM uses an accelerated electron beam to generate a light beam irradiated onto the sample surface, which then produces signals such as high-energy electron reflection, electron radiation, or X-rays. These signals are detected and analyzed by a detector [18]. The morphological characterization and elemental distribution of iron phases within the composite matrices were examined through high-resolution scanning electron microscopy. Imaging operations were conducted utilizing a Tescan MIRA LMS field-emission instrument manufactured in the Czech Republic. BC test conditions: scale 10 μm; content: morphology, requires gold sputtering. BC-nZVI test conditions: scale 2–10 μm; content: morphology, no gold sputtering required.

2.4.2 Fourier Transform Infrared Spectroscopy (FTIR)

Fourier-transform infrared spectroscopy represents an established analytical methodology for molecular-level identification of chemical constituents through detection of vibrational energy transitions. This technique exploits the phenomenon wherein covalently bonded atomic assemblies exhibiting infrared activity undergo alterations in electric dipole moments upon interaction with incident radiation in the infrared spectral region. The differential absorbance exhibited by distinct molecular moieties across the electromagnetic spectrum is graphically represented as a function of energy, conventionally expressed in reciprocal centimeters. Interpretation of characteristic absorption patterns enables elucidation of surface chemical functionality present on carbonized biomass substrates [19]. The present investigation employed spectral acquisition parameters encompassing a mid-infrared scanning window of 400–4000 cm^{-1} with 1 cm^{-1} resolution to generate vibrational fingerprints of the synthesized materials.

2.4.3 X-Ray Diffraction (XRD)

X-ray diffraction analysis serves as a predominant technique for investigating crystallographic properties encompassing atomic periodicity, spatial arrangement of constituent atoms, domain dimensions, and unit cell parameters. The methodology involves directing a collimated monochromatic X-ray beam toward a specimen positioned on a planar substrate at defined angular orientations. Upon specimen irradiation, characteristic intensity maxima and minima emerge at specific angular positions due to wave interference phenomena. At particular incidence geometries, constructive interference from elastically scattered radiation by periodically arranged atomic planes produces detectable intensity amplification. A mobile detector traverses an angular trajectory equivalent to the source rotation, recording these diffraction maxima for angular determination. Application of Bragg's relationship permits calculation of interplanar spacings from measured diffraction angles. Comprehensive interpretation of the resulting diffractogram yields insights regarding internal structural organization, morphological features, chemical constitution, and degree of crystalline order within the material [20].

2.4.4 Specific Surface Area Determination (BET)

Brunauer-Emmett-Teller analysis constitutes a prevalent methodology for quantifying surface area characteristics of porous substrates, encompassing numerous sorbent materials. The analytical protocol initiates with thermal pretreatment under reduced pressure to eliminate adsorbed volatile species from the specimen. The degassed sample is subsequently subjected to controlled exposure with an inert adsorptive—typically dinitrogen—maintained at cryogenic temperature, while the equilibrium relative pressure is systematically incremented across the complete range from zero to unity. Adsorbate molecules progressively accumulate within the porous architecture, initially occupying ultramicroporous voids followed by mesoporous channels and larger macroporous cavities, ultimately establishing a complete monomolecular layer across the entire accessible surface. Continued elevation of adsorptive pressure facilitates the development of successive multimolecular strata atop the initial monolayer coverage. The amount of gas adsorbed or the reverse process (desorption) is measured as a function of pressure. Theoretical frameworks such as the BET model enable calculation of surface area metrics and pore dimensional distributions that govern material functionality [21]. Enhanced interfacial area correlates directly with superior sorptive capacity. Dinitrogen was selected as the probe molecule for surface characterization of the catalytic materials in this investigation. Pretreatment conditions involved thermal desorption at 120°C for an eight-hour duration to ensure complete removal of physisorbed contaminants prior to analysis. The instrument model used was Quantachrome Nova 4000e.

3 Results and Discussion

3.1 Comparison of Performance of Different Materials

The performance of different materials was investigated, focusing on two main aspects: first, the degradation effect on tetracycline, which directly determines the basic performance of the material for pollutant degradation; second, the iron-loading capacity of the material, including iron loading amount and stability, which determines the material's ability to catalyze stably and continuously in the reaction system, directly affecting the degradation efficiency.

3.1.1 Degradation Experiments of Tetracycline by Different Materials in a Fenton-like System

The degradation of tetracycline by nine different materials is shown in Figure 1. It can be observed that for BC-nZVI materials using biochar prepared at different temperatures as the carrier, comparing the gradients of iron-to-carbon ratios.

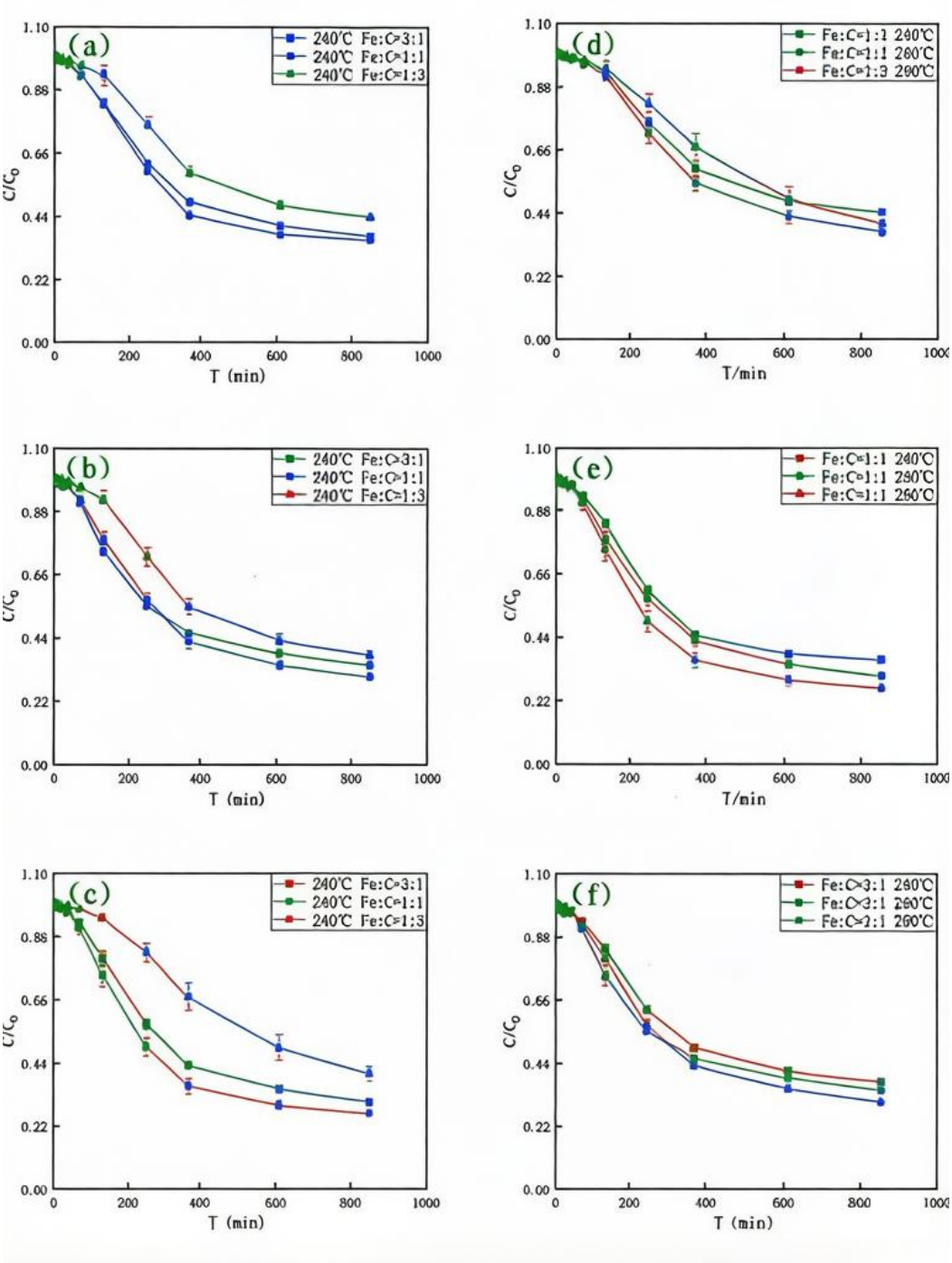

Figure 1 Comparison 0f degradation efrects of difrerent materials on tetracycline in Fenton- like system

For the three materials prepared at 240°C, with Fe:C ratios of 1:3, 1:1, and 3:1, the removal rates at equilibrium were 55.72%, 66.81%, and 62.79%, respectively. Among them, the material with Fe:C=1:1 showed better removal efficiency. For the three materials prepared at 260°C, with the same Fe:C ratios, the equilibrium removal rates

were 62.31%, 69.54%, and 65.58%, respectively. The material with Fe:C=1:1 again showed better removal efficiency. For the three materials prepared at 280°C, the equilibrium removal rates were 60.98%, 73.83%, and 69.83%, respectively. The material with Fe:C=1:1 demonstrated the best removal efficiency. Examination of the graphical data presented in panels a, b, and c reveals that across all three biochar preparation temperatures, the composite material formulated at an iron-to-carbon stoichiometry of 1:3 exhibited markedly inferior degradation efficacy relative to counterparts prepared at 1:1 and 3:1 ratios. This diminished performance stems from the reduced proportion of metallic iron within the hybrid structure, which translates to diminished surface density of redox-active centers and consequently attenuated catalytic activity. Simultaneously, when biochar is excessive, the biomass char itself may agglomerate and occupy the active sites of nZVI, reducing the activity of zero-valent iron, thereby decreasing the tetracycline degradation rate [22].

In contrast, the degradation effects of materials with Fe:C=1:1 were better. This is because the roles in the system include adsorption, reduction, and catalytic degradation. When Fe:C=1:1, nZVI is relatively uniformly distributed on the biochar, and the synergistic effect of adsorption, reductive degradation, and catalysis is maximized [23]. When the iron-to-carbon ratio is 3:1, nZVI is in excess, and the biochar's space is insufficient to accommodate it, leading to uneven distribution of nZVI on the biochar surface, agglomeration of most nZVI particles. Increased agglomeration reduces the specific surface area of nZVI participating in catalysis, thus leading to a decrease in degradation rate. From Figures e and f, it can be observed that as the biochar preparation temperature increases, the degradation efficiency of tetracycline by materials with Fe:C=1:1 and Fe:C=3:1 in the reaction system gradually enhances. Finally, the material with Fe:C=1:1 prepared at 280°C achieved a relatively high removal rate of 73.83% among the nine materials. This indicates that the composite material using biochar as a carrier has certain requirements for the iron-to-carbon ratio, and the preparation temperature has a greater impact on materials with low iron loading. When the iron-to-carbon ratio reaches 1:1 or higher, this influence manifests as enhanced material performance with increasing temperature, possibly because the preparation temperature of biochar affects the formation of its surface functional groups, including type and quantity. Elevated pyrolysis temperatures promote greater abundance of surface oxygenated functionalities [24], thereby enhancing the affinity of the carbonaceous matrix for metallic nanoparticle immobilization and ultimately yielding superior catalytic behavior.

Based on the material degradation experimental results, the BC-nZVI material with Fe:C=1:1 prepared at 280°C exhibited a high removal efficiency for tetracycline (73.83%) under the reaction system. Therefore, this material was selected for subsequent experiments.

3.1.2 Iron Loading Performance of Different Materials

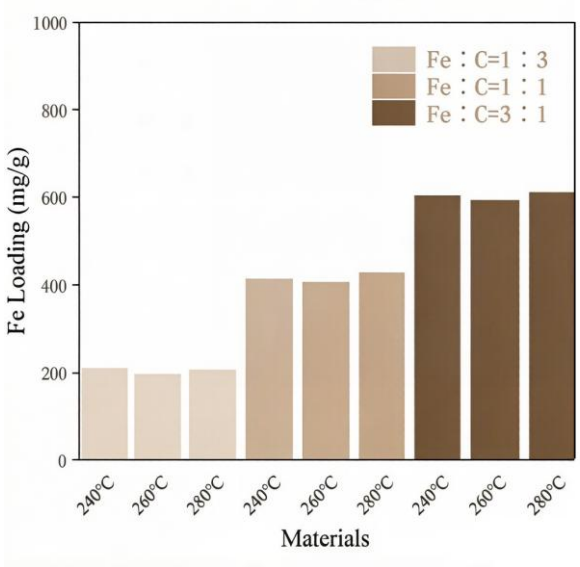

Figure 2 Fe loading of different materials

The iron loading of materials under different preparation conditions is shown in Figure 2. The iron loading capacities (mg/g) were as follows: 206.3, 194.8, 202.9, 412.6, 404.6, 426.5, 602.2, 590.7, 610.9. It can be seen that materials with Fe:C=3:1 have a higher iron loading capacity. However, from the difference in iron loading between the three iron-to-carbon ratio groups, the increase achieved by changing the ratio from 1:3 to 1:1 is greater than that from 1:1 to 3:1, indicating that when the iron-to-carbon ratio is greater than 1:1, the benefit of further increasing the iron dosage on the material's iron loading capacity gradually diminishes.

The physical stability of the materials is shown in Figure 3. The residual iron amounts (%) were as follows: 84.64, 78.40, 85.23, 93.02, 92.02, 93.92, 84.50, 88.29, 82.17. The figure shows that the three materials with Fe:C=1:1 have good physical stability. After 12 hours of oscillation in water, the residual iron loading remained above 90%. Among them, the BC-nZVI material with Fe:C=1:1 prepared at 280°C exhibited the best physical stability, with a residual iron loading of 93.92%. Tests on the six materials with Fe:C=1:3 and Fe:C=3:1 showed significantly poorer physical stability, with residual iron loadings only between 80% and 90%. For the three materials with Fe:C=1:3, this is due to the lower iron loading and poor loading effect (too dispersed), making surface iron prone to loss. For the three materials with Fe:C=3:1, the poor stability can be attributed to excessive iron loading, causing surface nZVI to agglomerate easily and not load well onto the carbon material, resulting in poor impact resistance and being easily washed away.

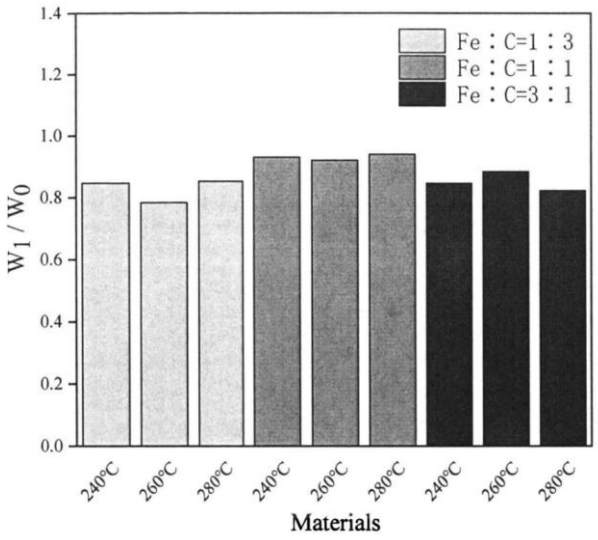

Figure 3 Residual Fe loading of different materials

The chemical stability is shown in Figure 4. The residual iron amounts (%) were as follows: 55.22, 52.87, 54.63, 61.73, 55.75, 64.19, 47.94, 47.41, 47.83. It can be seen that the three materials with Fe:C=1:1 also have good chemical stability. Under pH=2 conditions and oscillating for 12 hours, the residual iron loadings of materials prepared at 240°C and 280°C both exceeded 60%. The residual iron loading of materials with Fe:C=1:3 was between 50% and 60%, while that of the three materials with Fe:C=3:1 was only about 47%. This is because excessive iron loading leads to surplus nZVI that cannot be uniformly loaded on the biochar surface effectively, and the biochar lacks sufficient functional groups to bond with iron, causing most of the nZVI to be loosely covered on the surface in an agglomerated form, which is easily lost under acidic conditions.

DOI:

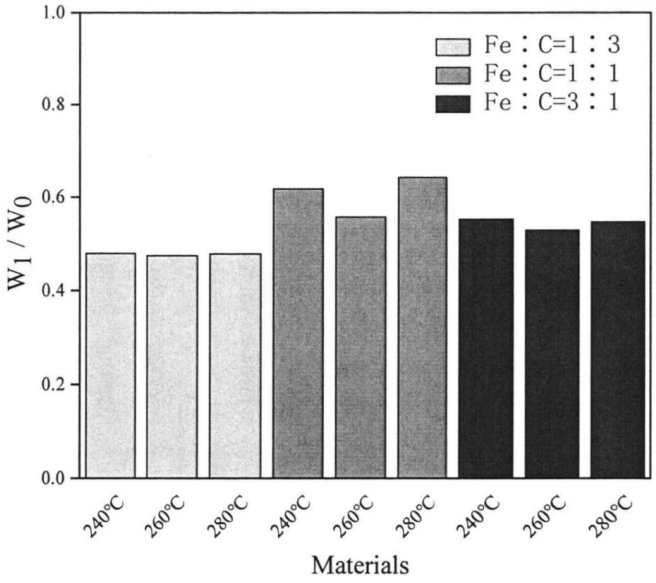

Figure 4 Residual Fe loading of different materials

Figure 5 shows the removal of tetracycline by BC-nZVI and nZVI, as well as the two materials after different numbers of reuse cycles, in the Fenton-like system. In the first use, the removal rates of tetracycline by BC-nZVI and nZVI under reaction conditions reached 95.12% and 95.84%, respectively. It can be observed that in the first four uses, both materials achieved tetracycline removal rates above 95% under the same reaction conditions, indicating that both have high removal efficiency for tetracycline within a short use cycle. After the fifth cycle of use, the removal rates of tetracycline by both materials in the reaction system began to decline to varying degrees. For both materials, this may be due to oxidation of the material to varying degrees with increasing number of cycles, reducing activity. Simultaneously, increased use cycles lead to decreased iron content and accumulation of tetracycline adsorbed by the material, which directly reduces degradation efficiency [25]. Meanwhile, compared to nZVI, BC-nZVI exhibited stronger stability, likely because biochar, as a carrier, can effectively disperse and fix nZVI particles, prevent material loss and oxidation, and increase the adsorption capacity for tetracycline.

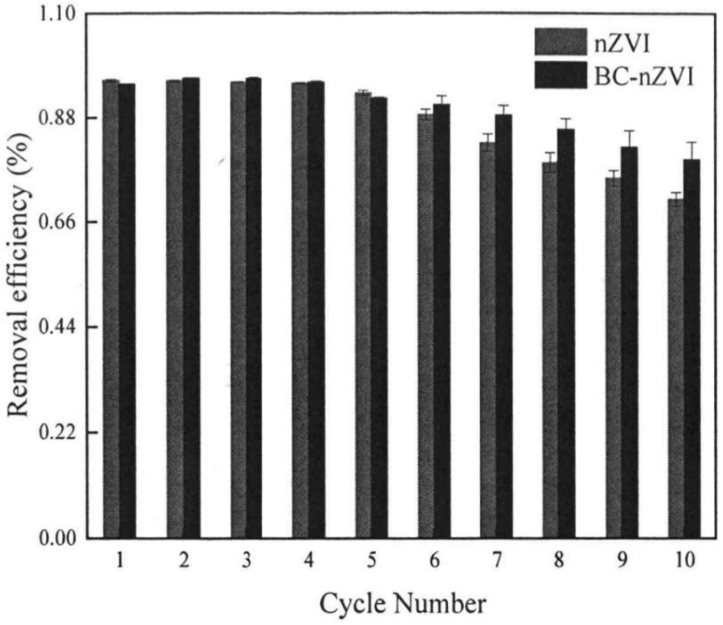

Figure 5 Comparison of degradation effcts of nZVI and BC-nZVI materials on tetracycline by recycling

As the number of cycles continued to increase, after 10 reuses, the removal rates of tetracycline by nZVI and BC-nZVI in the reaction system decreased by 25.16% and 16.07%, respectively, compared to the first use. However, the removal rate of BC-nZVI for tetracycline could still reach 79.05%, while that of nZVI was only 70.69%. The results indicate that the materials do not experience a significant performance decline or loss of tetracycline degradation ability during cyclic use, proving that BC-nZVI has strong catalytic capacity, adsorption performance, and stability in the Fenton-like system treatment. Related studies have also found that carbon carriers can greatly enhance the stability of zero-valent iron and strengthen reuse capability, showing broad application prospects. Zhang et al. [74] used mesoporous carbon-supported zero-valent iron to degrade sulfamethazine in a persulfate system. The degradation rate remained at 46.4% after 3 cycles of use. Li et al. [26] prepared iron-loaded materials from corn straw and cob biochar via impregnation for trichloroethylene degradation in an oxidation system. After 3 cycles, the degradation effect decreased from 100% to 80%, and a significant decline appeared during the fourth use, with the degradation rate dropping to 50%.

3.2 Structural Characterization and Analysis

3.2.1 Fourier Transform Infrared Spectroscopy (FTIR) Analysis

The vibrational spectra of the synthesized materials are presented in Figure 6. Spectral analysis of the pristine carbonized biomass reveals a prominent absorption band centered at 3410 cm^{-1}, attributable to the coupled stretching modes of alcoholic O-H moieties and ethereal C-O linkages. The peak around 2920 cm^{-1} is generated by C-H vibration. The characteristic peak generated by C=O stretching vibration is at 1740 cm^{-1}. The peak at 1625 cm^{-1} is attributed to the vibration of the aromatic hydrocarbon backbone. The peaks between 1022 cm^{-1} and 1264 cm^{-1} belong to the vibrations of aromatic derivatives, rings, and C-O stretching in cellulose and hemicellulose. These characteristic peaks demonstrate the generation of biochar [26]. The FTIR spectrum of BC-nZVI shows characteristic absorption peaks of Fe-OH-Fe and Fe-O around 600 cm^{-1} [17]. The appearance of these absorption peaks proves the successful loading of Fe onto the biochar.

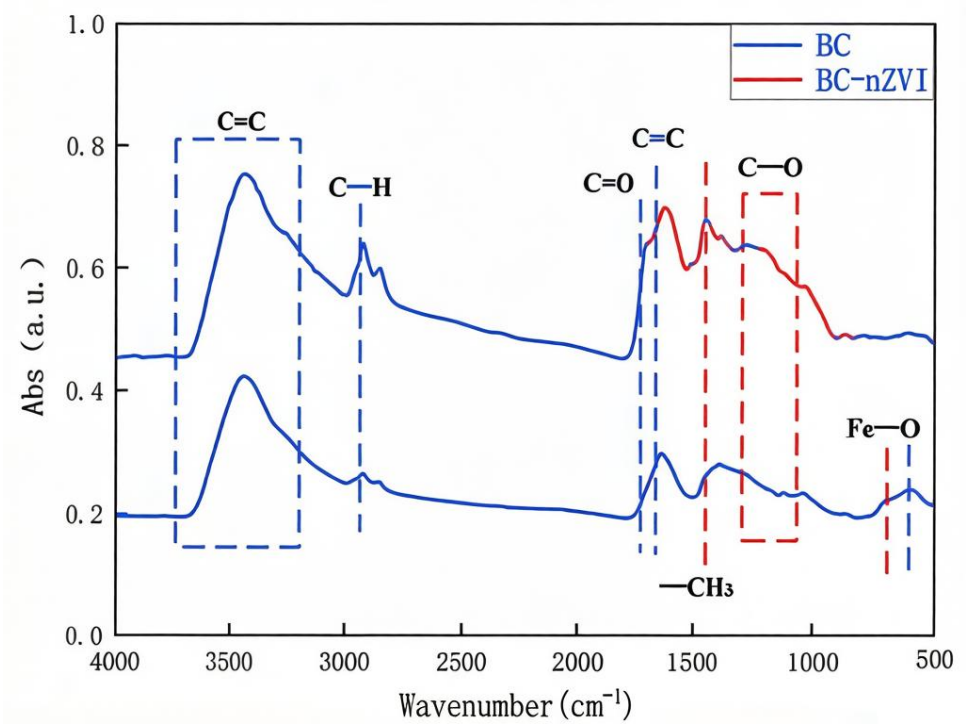

Figure 6 FTIR spectra of BC, BC-nZVI materials

3.2.2 Scanning Electron Microscopy (SEM) Analysis

The SEM images of biochar (BC) are shown in Figure 7. The SEM images of the BC-nZVI materials are shown in Figure 8.

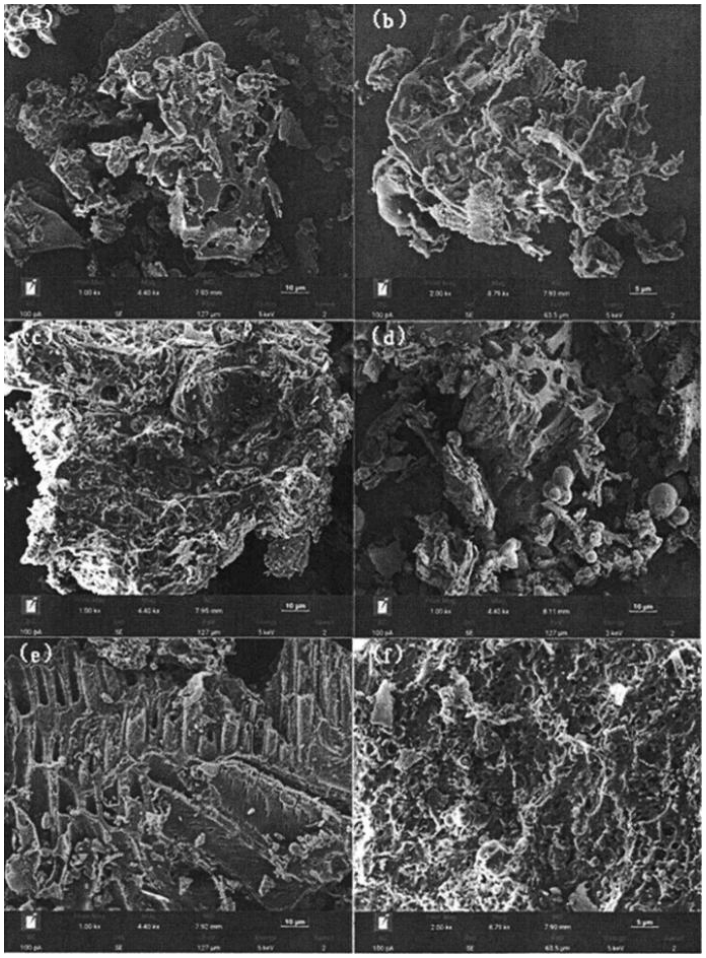

Figure 7 SEM images of BC

Figure 7 shows that the biochar structure is very complex, irregular in shape, and rich in pores. These factors determine that biochar has a large specific surface area. The rough biochar surface and large specific surface area are also conducive to the loading of zero-valent iron [16]. Figures 8 (a) and (d) correspond to BC-nZVI material with an iron-to-carbon ratio of 3:1; (b) and (e) correspond to BC-nZVI with a ratio of 1:1; (c) and (f) correspond to BC-nZVI with a ratio of 1:3. A large number of spherical zero-valent iron particles with diameters below 100 nm are observed attached to the biochar surface. It can be seen that the zero-valent iron on the surface of the BC-nZVI material with Fe:C=3:1 is surplus and tends to agglomerate in excess areas, resulting in less-than-ideal local loading. The zero-valent iron on the surface of the BC-nZVI material with Fe:C=1:1 is relatively uniformly and densely distributed. Upon local magnification, it can be seen that the zero-valent iron is well loaded on the biochar and not prone to agglomeration. In contrast, the overall iron loading amount of the BC-nZVI material with Fe:C=1:3 is relatively low, the distribution is sparse, and large areas of biochar are exposed, indicating poor zero-valent iron loading. Zhang et al. [18] also found that the agglomeration of nanoscale zero-valent iron was well alleviated due to the presence of biochar, but excessive zero-valent iron would lead to aggravated agglomeration because the active sites on biochar are limited and nZVI particles are extremely small; agglomeration occurs when the binding force exceeds their own weight.

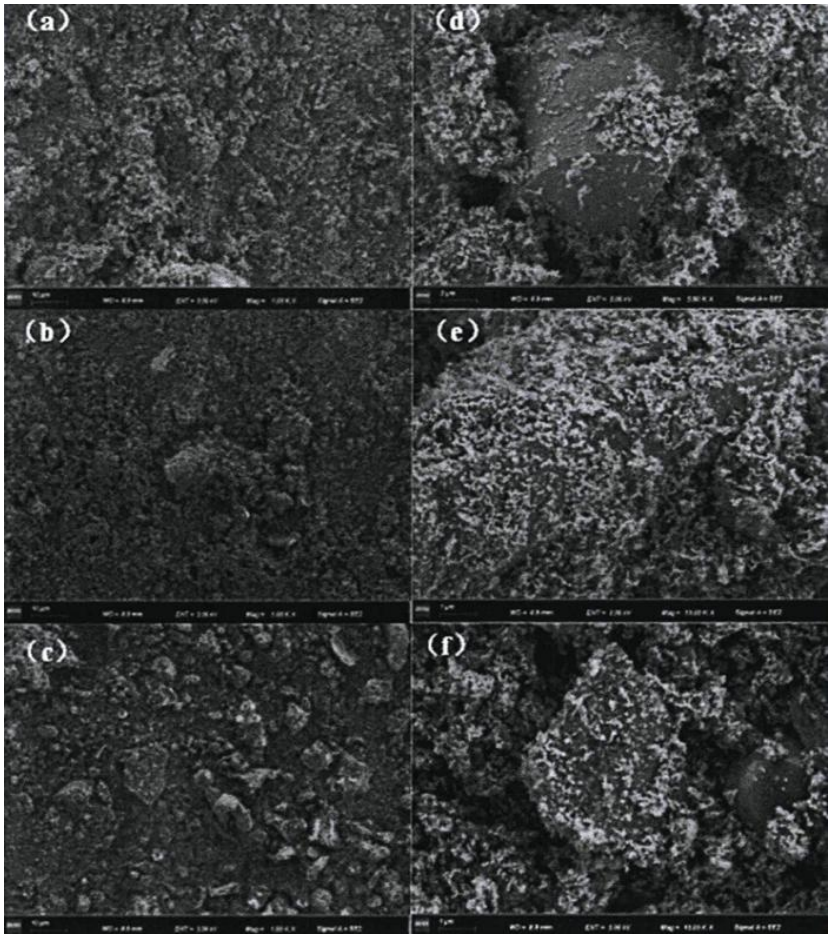

Figure 8 SEM images of BC-nZVI (a) Fe:C=3:1 280°C, magnification 1 000 times (b) Fe: C=1:1 280°C, magnification 1000 times (c) Fe:C=1:3 280°C, magnincation 1000 times (d) Fe:C=3:1 280°C, magnincation 5000 times (e) Fe:C=1:1 280°C, magnincation 5000 times (f) Fe:C=1:3 280°C， magnincation 5000 times

3.2.3 X-Ray Diffraction (XRD) Analysis

Crystalline phase testing of powdered samples of BC and BC-nZVI materials was performed using an X-ray diffractometer. The test patterns are shown in Figure 9, showing diffraction peaks of the samples at specific positions. Around 2θ = 20°, the original BC shows a unique broad XRD peak, indicating the presence of an amorphous graphitic structure [19]. The diffraction peak in the BC-nZVI material test pattern at 2θ = 45.32° provides evidence for the presence of α-Fe^0, indicating that nZVI was successfully prepared by the liquid-phase reduction method [20]. The standard 2θ diffraction angle for Fe^0 is 44.90°. The expanded angular position of the metallic iron reflection suggests perturbation of the zerovalent iron crystalline arrangement by the carbonaceous support matrix, while conversely, the incorporation of metallic nanoparticles disrupts the inherent graphitic ordering of the biochar substrate. The presence of diffuse, non-discrete scattering features indicates the existence of iron in a non-crystalline state, attributable to the intrinsically poor structural organization characteristic of highly reactive nanoscale zerovalent species exhibiting substantial reductive capacity and sorptive affinity [27].

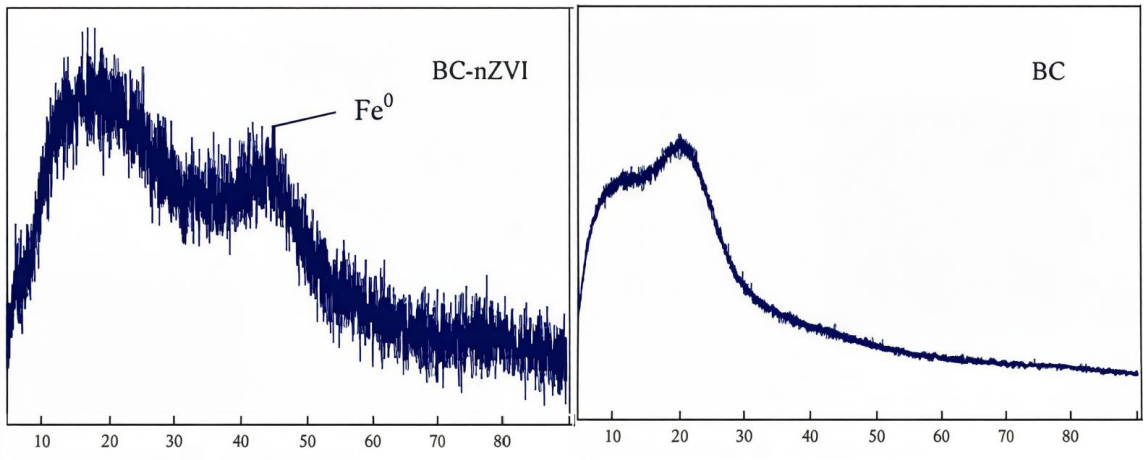

Figure 9 XRD spectra of BC，BC-nZVI

3.2.4 Specific Surface Area Determination (BET)

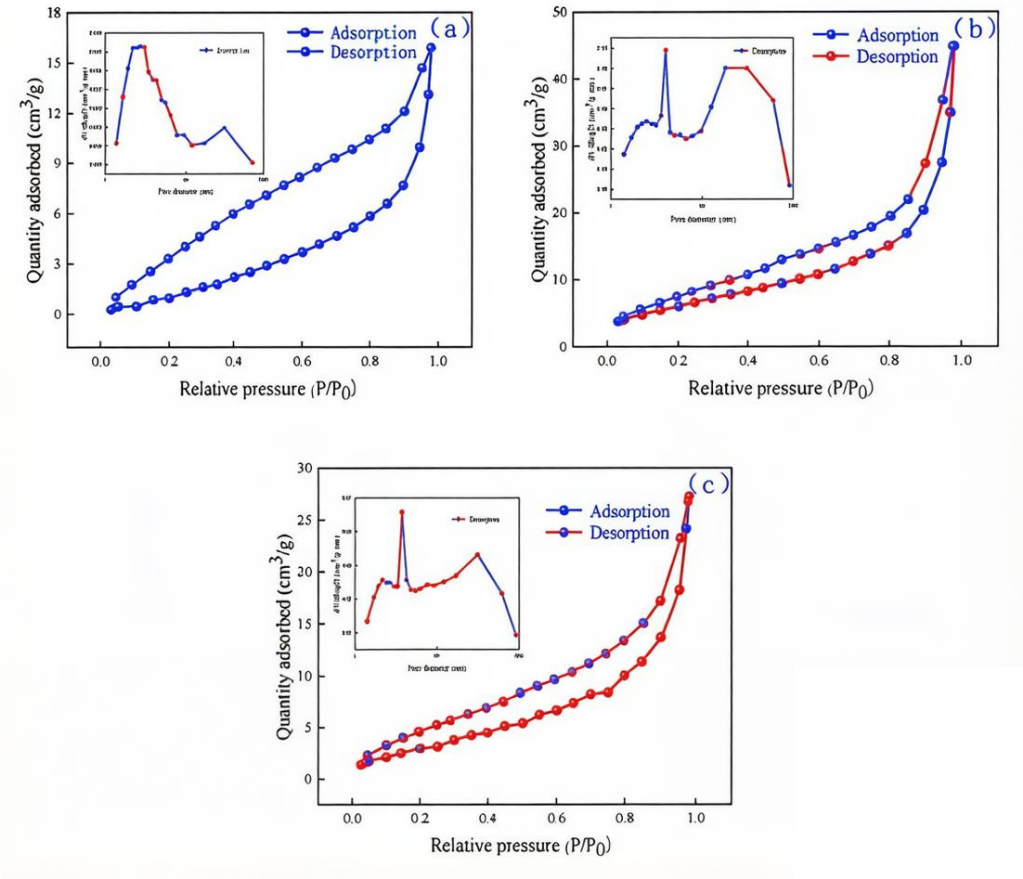

Figure 10 N2 adsorption desorption curves of different materials (a) BC (b) nZvI (c) BC-nZVI

The N_2 sorption isotherms and corresponding textural parameters for the carbonized biomass, nanoscale zerovalent iron, and their hybrid composite are illustrated in Figure 3.10. All three specimens exhibit Type IV adsorption profiles with H3 hysteresis characteristics, signifying the coexistence of microporous and mesoporous architectures within both the pristine biochar and the iron-impregnated composite, with mean pore apertures centered around 1.2 nm. Prior investigations demonstrate that hydrothermal processing induces biomass depolymerization into lower molecular weight fragments, generating additional porosity on the carbonaceous

surface and consequently amplifying the accessible interfacial area. Nevertheless, excessive thermal elevation during hydrothermal treatment proves detrimental to surface area development. Concurrently, the void volume within the carbonized biomass exhibits strong correlation with its surface area characteristics [28]. The dimensional attributes of these pores serve to effectively mitigate particle aggregation phenomena associated with metallic iron nanophases [29], thereby conferring upon the composite material diminished iron crystallite dimensions and consequently maximal catalytic efficacy. The specific surface areas of biochar, nZVI, and BC-nZVI materials are 31.22 m^2/g, 41.82 m^2/g, and 30.78 m^2/g, respectively. After loading zero-valent iron, the specific surface area of the BC-nZVI material decreases compared to biochar, and the pore size also decreases from 1.81 nm to 1.49 nm. This is because after impregnation, zero-valent iron precipitates on the biochar surface or embeds into the pores, causing blockage [30].

Based on the experimental data and characterization results presented in the document, the degradation mechanism of tetracycline (TC) by the biochar-supported nanoscale zero-valent iron (BC-nZVI) composite within the Fenton-like system is a complex, synergistic process involving adsorption, chemical reduction, and radical-based catalytic oxidation, all facilitated by the unique structural and chemical properties of the composite material. The mechanism initiates with the rapid adsorption of TC molecules onto the BC-nZVI surface, primarily driven by the large specific surface area (30.78 m^2/g for the optimal composite), the intricate porous structure of the biochar carrier (with pores around 1.49 nm as per BET analysis), and potential interactions such as π-π stacking between TC's aromatic rings and the graphitic domains of biochar, as well as hydrogen bonding with surface oxygen-containing functional groups (e.g., -OH, C=O identified by FTIR at ~3410 cm^{-1} and 1740 cm^{-1}). This preconcentration of pollutants near the active sites significantly enhances the subsequent degradation efficiency. The core catalytic cycle is driven by the nanoscale zero-valent iron (nZVI) particles, which are uniformly distributed on the biochar surface in the optimal Fe:C=1:1 material (as confirmed by SEM, contrasting with agglomeration at Fe:C=3:1). In the acidic or near-neutral aqueous environment, the nZVI (Fe^0) corrodes, releasing Fe^{2+} ions ($Fe^0 + 2H^+ \rightarrow Fe^{2+} + H_2$). These Fe^{2+} ions then catalyze the decomposition of the added H_2O_2 via the classical Fenton reaction ($Fe^{2+} + H_2O_2 \rightarrow Fe^{3+} + \cdot OH + OH^-$), generating highly reactive hydroxyl radicals (·OH), the presence of which is directly evidenced by Electron Paramagnetic Resonance (EPR) analysis. The generated Fe^{3+} can be reduced back to Fe^{2+} either by additional surface-bound Fe^0 ($2Fe^{3+} + Fe^0 \rightarrow 3Fe^{2+}$) or by reaction with hydroperoxyl radicals ($HO_2\cdot$) produced from ·OH scavenging ($Fe^{3+} + HO_2\cdot \rightarrow Fe^{2+} + O_2 + H^+$), thus establishing a sustainable catalytic cycle that continuously produces ·OH radicals. Concurrently, the nZVI itself can directly reduce certain functional groups of TC through electron transfer, contributing to its decomposition. The biochar support plays a multifaceted role beyond mere adsorption: it prevents the agglomeration and loss of nZVI nanoparticles, thereby maintaining a high density of active sites and enhancing material stability—this is reflected in the superior reusability where BC-nZVI retained a 79.05% removal rate after 10 cycles compared to 70.69% for bare nZVI. Furthermore, the biochar's conductive carbon matrix may facilitate electron transfer between $Fe^0/Fe^{2+}/Fe^{3+}$ species, potentially accelerating the redox cycles. The generated ·OH radicals non-selectively attack the TC molecule, leading to a series of oxidative transformations. As inferred from LC-MS analysis of degradation intermediates, the pathway likely involves hydroxylation of the aromatic rings, demethylation of $-N(CH_3)_2$ groups, cleavage of the $CONH_2$ group, and subsequent ring-opening reactions of the naphthacene core structure. These processes break down the complex TC molecule into smaller, less refractory organic acids and aldehydes, ultimately leading to profound mineralization into CO_2 and H_2O, as substantiated by the high Total Organic Carbon (TOC) removal rate of 81.63%. The synergy is paramount: biochar efficiently concentrates TC and stabilizes the catalyst, while the dispersed nZVI provides a persistent source of Fe^{2+} for H_2O_2 activation. The optimal performance at Fe:C=1:1 and a biochar preparation temperature of 280°C stems from this balance, ensuring sufficient iron loading for catalysis without causing nanoparticle aggregation (which reduces active surface area) while the higher pyrolysis temperature enriches the biochar with functional groups beneficial for both pollutant interaction and iron anchoring. The mechanism can be visually summarized in a conceptual diagram depicting: (1) TC molecules diffusing and adsorbing onto the porous biochar structure with embedded nZVI particles; (2) Fe^0 corrosion and Fe^{2+} release at the solid-liquid interface; (3) H_2O_2 activation at Fe^{2+} sites producing ·OH radicals; (4) ·OH radicals attacking the adsorbed TC molecule, leading to its structural breakdown via hydroxylation, demethylation, and ring-opening; (5) Regeneration of Fe^{2+} from Fe^{3+} via reaction with Fe^0 or radical species, closing the catalytic loop; and (6) Final emission of CO_2 and H_2O from the mineralized products.

Conclusion

This work prepared biochar under three different temperature conditions (240°C, 260°C, 280°C) via hydrothermal carbonization. Based on this, nine different BC-nZVI composite materials were prepared using the liquid-phase reduction method by varying the iron-to-carbon ratio (Fe:C=1:3, 1:1, 3:1). These specimens were deployed for tetracycline abatement studies within a Fenton-inspired oxidation framework. Subsequent evaluation of iron retention capacity was conducted, with pre- and post-reaction metallic content determined through aqueous agitation and pH modification protocols to assess the structural and chemical robustness of the materials. The regenerative capacity of the synthesized materials was evaluated through sequential reuse trials. Comprehensive characterization of surface chemistry, topographical features, crystallographic arrangement, interfacial area, and graphitization extent was subsequently performed employing vibrational spectroscopy, electron microscopy, X-ray diffraction, and gas sorption analysis. The analysis results are as follows:

When the iron-to-carbon ratio of the BC-nZVI composite material is 1:3, the degradation rate is low due to low iron loading, most iron being within the pore structure of the biochar, and possible agglomeration of biochar affecting nZVI activity. When the iron-to-carbon ratio reaches 1:1, with the increase in iron loading, a sufficient amount of nZVI participates in the reaction, the influence of adsorption and mass transfer by biochar on the degradation rate gradually weakens, the impact of biochar preparation temperature on material performance begins to weaken, and the synergistic effect of adsorption, reductive degradation, and catalysis reaches its maximum. When the iron-to-carbon ratio is 3:1, the degradation rate decreases due to agglomeration of nZVI. At a pyrolysis temperature of 280°C with equimolar iron-to-carbon stoichiometry, the metallic iron phase exhibited homogeneous dispersion across the carbonaceous substrate, yielding degradation efficiencies superior to the majority of the nine formulations examined. This particular composite was designated for further investigative procedures.

The iron loading capacities of the nine BC-nZVI materials were tested. Residual iron loading was used to represent the physical and chemical stability of the materials. When the iron-to-carbon ratio is 1:1, the nZVI is relatively uniformly distributed on the biochar surface with good loading effect, resulting in the best physical and chemical stability of the materials. When the iron-to-carbon ratio is 3:1, due to severe agglomeration of surplus zero-valent iron, which cannot load well on the biochar, both physical and chemical stability are poor. Among the nine materials, the BC-nZVI material with Fe:C=1:1 prepared at 280°C exhibited good physical and chemical stability, with residual iron loadings of 93.92% and 64.19%, respectively.

Cycling experiments on the materials showed that the tetracycline removal rate could still reach 79.05% after ten uses, demonstrating good reusability and stability of the material.

Analytical investigations employing vibrational spectroscopy, electron microscopy, X-ray diffraction, and gas sorption methodologies confirmed the carbonized biomass exhibits irregular surface topography, abundant porosity, substantial interfacial area, and diverse chemical functionality. Spectral evidence revealed iron-specific absorption signatures, while diffractometric analysis detected characteristic reflections attributable to metallic iron phases, substantiating successful immobilization of nanoscale zerovalent species onto the biochar matrix concomitant with disruption of the native graphitic ordering. Furthermore, SEM images showed that nZVI on the surface of BC-nZVI material with Fe:C=3:1 is prone to agglomeration; the nZVI loading amount on the material with Fe:C=1:3 is low, with large areas of biochar exposed; and the nZVI on the surface of BC-nZVI material with Fe:C=1:1 is relatively uniformly and densely distributed, indicating a good loading effect.

References

[1] SCARIA J, ANUPAMA K V, NIDHEESH P V. Tetracyclines in the environment: An overview on the occurrence, fate, toxicity, detection, removal methods, and sludge management[J]. Sci Total Environ, 2021, 771: 145291.
[2] ZHU H, CHEN T, LIU J, et al. Adsorption of tetracycline antibiotics from an aqueous solution onto graphene oxide/calcium alginate composite fibers[J]. RSC Adv, 2018, 8(5): 2616-21.
[3] PULICHARLA R, BRAR S K, ROUISSI T, et al. Degradation of chlortetracycline in wastewater sludge by ultrasonication, Fenton oxidation, and ferro-sonication[J]. Ultrason Sonochem, 2017, 34: 332-42.
[4] XU L, ZHANG H, XIONG P, et al. Occurrence, fate, and risk assessment of typical tetracycline antibiotics in

the aquatic environment: A review[J]. Sci Total Environ, 2021, 753: 141975.
[5] CHEN J, LI H, LI J, et al. Efficient removal of tetracycline from water by tannic acid-modified rice straw-derived biochar: Kinetics and mechanisms[J]. Journal of Molecular Liquids, 2021, 340: 117237.
[6] KIM Y, LEE K B, CHOI K. Effect of runoff discharge on the environmental levels of 13 veterinary antibiotics: A case study of Han River and Kyungahn Stream, South Korea[J]. Mar Pollut Bull, 2016, 107(1): 347-54.
[7] NANTABA F, WASSWA J, KYLIN H, et al. Occurrence, distribution, and ecotoxicological risk assessment of selected pharmaceutical compounds in water from Lake Victoria, Uganda[J]. Chemosphere, 2020, 239: 124642.
[8] WANG Z, CHEN Q, ZHANG J, et al. Characterization and source identification of tetracycline antibiotics in the drinking water sources of the lower Yangtze River[J]. J Environ Manage, 2019, 244: 13-22.
[9] ALOTHMAN Z A, ALMASOUD N, MBIANDA X Y, et al. Synthesis and characterization of y-cyclodextrin-graphene oxide nanocomposite: Sorption, kinetics, thermodynamics and simulation studies of tetracycline and chlortetracycline antibiotics removal in water[J]. Journal of Molecular Liquids, 2022, 345: 116993.
[10] KOVALAKOVA P, CIZMAS L, MCDONALD T J, et al. Occurrence and toxicity of antibiotics in the aquatic environment: A review[J]. Chemosphere, 2020, 251: 126351.
[11] LAN L, KONG X, SUN H, et al. High removal efficiency of antibiotic resistance genes in swine wastewater via nanofiltration and reverse osmosis processes[J]. J Environ Manage, 2019, 231: 439-45.
[12] PANDELE A M, IOVU H, ORBECI C, et al. Surface modified cellulose acetate membranes for the reactive retention of tetracycline[J]. Separation and Purification Technology, 2020, 249: 117145.
[13] CHEN X, YANG Y, KE Y, et al. A comprehensive review on biodegradation of tetracyclines: Current research progress and prospect[J]. Sci Total Environ, 2022, 814: 152852.
[14] LIAO Q, RONG H, ZHAO M, et al. Interaction between tetracycline and microorganisms during wastewater treatment: A review[J]. Sci Total Environ, 2021, 757: 143981.
[15] SONG X, LIU R, CHEN L, et al. Comparative experiment on treating digested piggery wastewater with a biofilm MBR and conventional MBR: simultaneous removal of nitrogen and antibiotics[J]. Frontiers of Environmental Science & Engineering, 2017, 11(2): 1-9.
[16] PENG X, CAO J, XIE B, et al. Evaluation of degradation behavior over tetracycline hydrochloride by microbial electrochemical technology: Performance, kinetics, and microbial communities[J]. Ecotoxicology and Environmental Safety, 2020, 188: 109869.
[17] YANG P, YE Y, YAN Z, et al. Efficient removal of tetracycline in water by a novel chemical and biological coupled system with non-woven cotton fabric as carrier[J]. Chinese Chemical Letters, 2021, 32(9): 2823-7.
[18] ABBASNIA A, ZAREI A, YEGANEH M, et al. Removal of tetracycline antibiotics by adsorption and photocatalytic-degradation processes in aqueous solutions using metal organic frameworks (MOFs): A systematic review[J]. Inorganic Chemistry Communications, 2022, 145: 109959.
[19] BISWAL B K, BALASUBRAMANIAN R. Adsorptive removal of sulfonamides, tetracyclines and quinolones from wastewater and water using carbon-based materials: Recent developments and future directions[J]. Journal of Cleaner Production, 2022, 349: 131421.
[20] ZHAO J, GAO F, SUN Y, et al. New use for biochar derived from bovine manure for tetracycline removal[J]. Journal of Environmental Chemical Engineering, 2021, 9(4): 105585.
[21] HUANG Z, FANG X, WANG S, et al. Effects of KMnO4 pre- and post-treatments on biochar properties and its adsorption of tetracycline[J]. Journal of Molecular Liquids, 2023, 373: 121257.
[22] SCARIA J, NIDHEESH P V. Comparison of hydroxyl-radical-based advanced oxidation processes with sulfate radical-based advanced oxidation processes[J]. Current Opinion in Chemical Engineering, 2022, 36: 100830.
[23] MA D, YI H, LAI C, et al. Critical review of advanced oxidation processes in organic wastewater treatment[J]. Chemosphere, 2021, 275: 130104.
[24] AZFAR SHAIDA M, VERMA S, TALUKDAR S, et al. Critical analysis of the role of various iron-based heterogeneous catalysts for advanced oxidation processes: A state of the art review[J]. Journal of Molecular Liquids, 2023, 374: 121259.
[25] LI S, WU Y, ZHENG H, et al. Antibiotics degradation by advanced oxidation process (AOPs): Recent advances in ecotoxicity and antibiotic-resistance genes induction of degradation products[J]. Chemosphere, 2022, 311(Pt 2): 136977.
[26] MIYATA M, IHARA I, YOSHID G, et al. Electrochemical oxidation of tetracycline antibiotics using a Ti/IrO2 anode for wastewater treatment of animal husbandry[J]. Water Sci Technol, 2011, 63(3): 456-61.
[27] CHEN H, WANG J. Degradation and mineralization of ofloxacin by ozonation and peroxone (O3/H2O2) process[J]. Chemosphere, 2021, 269: 128775.

[28] GHASEMI H, MOZAFFARI S, MOUSAVI S H, et al. Decolorization of wastewater by heterogeneous Fenton reaction using MnO2-Fe3O4/CuO hybrid catalysts[J]. Journal of Environmental Chemical Engineering, 2021, 9(2): 105091.

[29] CHENG M, ZENG G, HUANG D, et al. Efficient degradation of sulfamethazine in simulated and real wastewater at slightly basic pH values using Co-SAM-SCS / H2O2 Fenton-like system[J]. Water Res, 2018, 138: 7-18.

[30] JIANG Y, RAN J, MAO K, et al. Recent progress in Fenton/Fenton-like reactions for the removal of antibiotics in aqueous environments[J]. Ecotoxicol Environ Saf, 2022, 236: 113464.